J. Biochem. **137**, 633–641 (2005)
DOI: 10.1093/jb/mvi077

Phospho-Pivot Modeling Predicts Specific Interactions of Protein Phosphatase-1 with a Phospho-Inhibitor Protein CPI-17

Fumiko Matsuzawa[1], Sei-ich Aikawa[1], Shin-ya Ohki[2] and Masumi Eto[3,*]

[1]Celestar Lexico-Sciences, Inc, MTG D17, Chiba 261-8501; [2]Japan Advanced Institute of Science and Technology (JAIST), Ishikawa 923-1292; and [3]University of Virginia School of Medicine, Center for Cell Signaling and Department of Molecular Physiology and Biological Physics, Charlottesville, VA22908-0577, USA

Received December 1, 2004; accepted March 7, 2005

Phospho-amino acids in proteins are directly associated with phospho-receptor proteins, including protein phosphatases. Here we produced and tested a scheme for docking together interacting phospho-proteins whose monomeric 3D structures were known. The phosphate of calyculin A, an inhibitor for protein phosphatase-1 and 2A (PP1 and PP2A), or phospho-CPI-17, a PP1-specific inhibitor protein, was docked at the active site of PP1. First, a library of 186,624 virtual complexes was generated *in silico*, by pivoting the phospho-ligand at the phosphorus atom by step every 5° on three rotational axes. These models were then graded for probability according to atomic proximity between two molecules. The predicted structure of PP1·calyculin A complex fitted to the crystal structure with r.m.s.d. of 0.23 Å, providing a validate test of the modeling method. Modeling of PP1·phospho-CPI-17 complex yielded one converged structure. The segment of CPI-17 around phospho-Thr38 is predicted to fit in the active site of PP1. Positive charges at Arg33/36 of CPI-17 are in close proximity to Glu274 of PP1, where the sequence is unique among Ser/Thr phosphatases. Single mutations of these residues in PP1 reduced the affinity against phospho-CPI-17. Thus, the interface of the PP1·CPI-17 complex predicted by the phospho-pivot modeling accounts for the specificity of CPI-17 against PP1.

Key words: cerebellar memory, computational simulation, hypertension, protein phosphorylation, myosin phosphatase, smooth muscle.

Abbreviations: PKC, Protein kinase C; ROCK, Rho-associated coiled-coil containing protein kinase; PP1, protein phosphatase-1; CPI-17, PKC-phosphorylated PP1 inhibitor (17 kDa); MYPT1, myosin-targeting subunit 1 of myosin phosphatase; GST, glutathione S-transferase; ATPγS, adenosine 5′-[γ-thio]triphosphate; r.m.s.d., root-mean-square deviation.

Protein–protein interaction is a fundamental process in cellular signal transduction. Phosphorylation of Ser/Thr as well as Tyr is often found at the molecular interface between molecules. The recognition involves binding of specific domains, such as 14-3-3, FHA, and SH2 (*1*, *2*). High-throughput methodology in structural biology accumulates 3D-structural data of known and anonymous proteins, and recent challenges in structural biology are to reveal 3D-structure of multi-protein complexes (*3*). Yet, structural information of protein complexes is still limited, compared with monomeric proteins, because of technical difficulties, such as stability of complexes in crystals. In parallel to structural biology, interactome projects, including large scale yeast-two hybrid screenings are uncovering entire networks of protein–protein interactions in yeast, fruit fly and *Caenorhabditis elegans* (*4*–*7*). Prediction of protein–protein interactions is the next step in this challenge of structural/functional proteomics.

Computer simulation is a powerful tool for prediction and analysis of protein–protein interactions (reviewed in Refs. *8* and *9*). Generally, the first stage of the prediction is to search docking interfaces in two proteins, where shapes of molecules are transformed to voxel grids, and virtual complexes are generated *in silico*. The second stage is scoring each interaction of the virtual complexes based on predefined parameters, such as van del Waal's and/or electrostatic interactions. Therefore, final models largely rely on the initial position of the ligand at the docking site. Algorithms for the prediction have been updated by adding new structural constraints obtained from experimental results, and successfully predicted structures of protein complexes (*8*, *10*–*13*). Yet, as the simulation comes into detail with increased information, it usually requires days-long computation using computers equipped with a high power processor and/or multiple processors.

Two abundant Ser/Thr phosphatases, protein phosphatase-1 (PP1) and protein phosphatase 2A (PP2A), consist of a bi-metal active site in the highly conserved catalytic domain (*14*). PP1 activity is regulated by the interaction with regulatory subunits as well as with phospho-inhibitor proteins (*15*). Because the phosphoester is labile on Ser/Thr phosphatases, there is no information on PP1/PP2A structures complexed with phospho-substrates or phospho-inhibitor proteins. CPI-17, a protein kinase C-phosphorylated inhibitor for myosin phosphatase, 17 kDa, is necessary for the regulation of

*To whom correspondence should be addressed. Phone: +1-434-982-0812, Fax: +1-434-243-2829, E-mail: me2h@virginia.edu

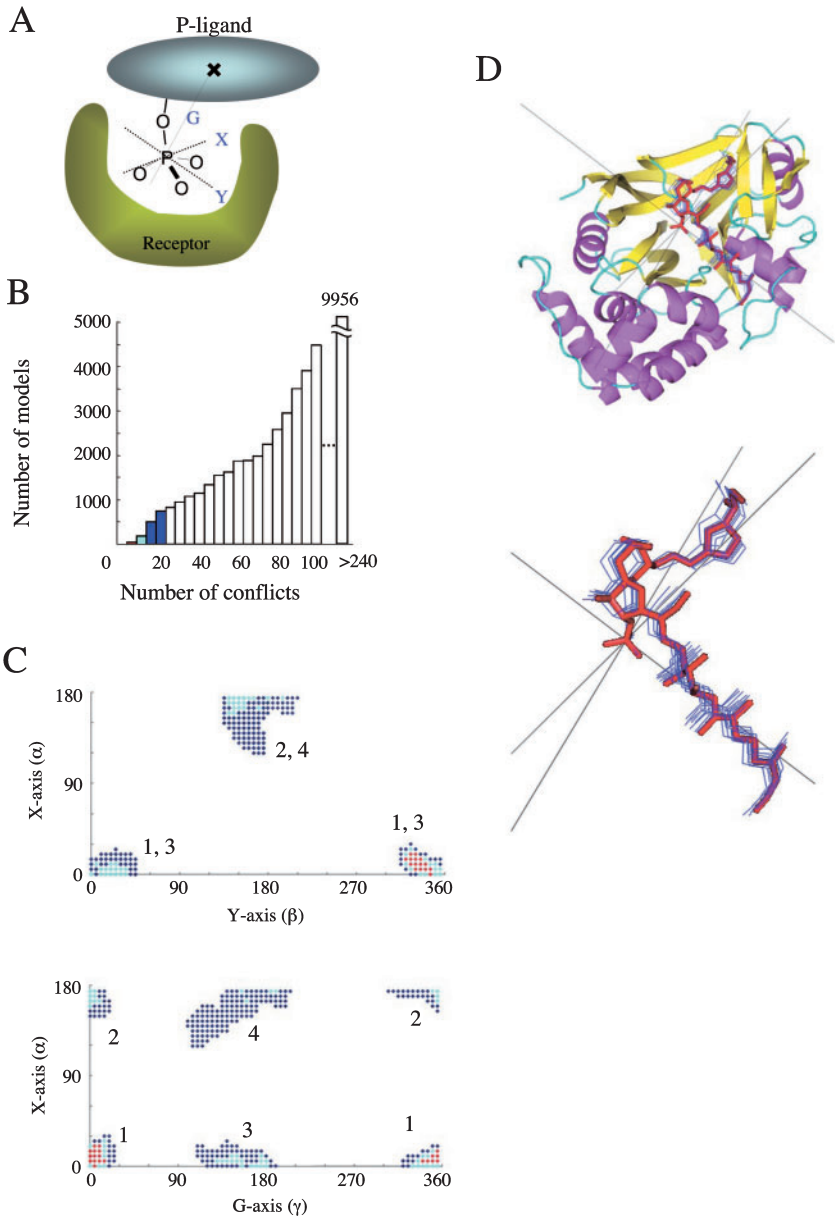

Fig. 1. **Phospho-pivot modeling of PP1·calyculin A complex.** (A) Three axes defined in the phospho-pivot modeling. (B) Distribution of models in conflict number. Models are classified by their number of conflicts. Red, cyan and blue bars indicate models with conflict number of 1–5, 6–10, and 11–20, respectively. (C) Distribution of models in angle map. A model is spotted as a dot against the angle of X/Y axes (top) and of X/G axes (bottom). Color of the dot indicates number of conflicts, as in panel B. Numbers on clusters correspond to the number in Table 1. (D) Superimposed image of PP1·calyculin A. Positions of calyculin A in top 10 models with conflict number of less than 2 (blue thin line) are superimposed to the crystal structure of the complex where calyculin A is indicated red thick line. The gray thin lines indicate the axes of rotation. The structure was drawn using PyMoL (*43*).

vascular smooth muscle contractility and for maintaining long-term synaptic depression of cerebellar Purkinje cells (*16–19*). CPI-17 is composed of a four-helix bundle, followed by a loop structure called inhibitory P-loop, where includes a critical phosphorylation site (Thr38) conferring inhibitory potency (*20*). Thr38 phosphorylation by PKC or ROCK triggers a conformational change of CPI-17 that converts it into a potent PP1- and myosin phosphatase-specific inhibitor (*21*, *22*). Other forms of PP1 can dephosphorylate and inactivate P-CPI-17, thereby P-CPI-17 specifically regulates myosin phosphatase in cells (*23*). Substitution of Thr38 with Asp causes a chemical shift perturbation in the NMR spectrum, similar to that resulting from the phosphorylation, due to the inhibitory P-loop becoming exposed to solvent (*24*). Therefore, the hypothesis is that the phosphate at Thr38 of CPI-17 docks directly at the active site of PP1 in myosin phosphatase, as a competitive inhibitor. Here we developed an algorithm to predict the structure of protein complexes, termed phospho-pivot modeling. The predicted PP1·P-CPI-17 interaction was tested by mutation of PP1, and the results support specificity of P-CPI-17 toward PP1 among Ser/Thr phosphatases.

EXPERIMENTAL PROCEDURES

Phosphate-Pivot Modeling—The structural coordinates of PP1 and calyculin A were individually extracted from data of the PP1·calyculin A crystal structure (PDB: 1IT6), and saved as PDB files. P-CPI-17 structure was virtually created from the structural data of T38D CPI-17(*22*–120) (PDB: 1J2N). Asp38 in T38D CPI-17 (residue 31–120) was substituted to phospho-Thr using SYBYL/BIOPOLYMER software (Tripos Inc. St. Louis, MO). The N-terminal 11 residues of CPI-17(*22*–120) were omitted from the modeling, because the structure of this portion is highly flexible. The phosphorus atom in ligands was positioned at that in PP1·calyculin A crystal structure,

and was used as a pivot. A line passing through the phosphorus atom and the geometrical center of phospho-ligands (labeled × in Fig. 1A) was defined rotational axis *G*, which is variable against other axes. A fixed rectangular axis for rotation, *X* and *Y*, was set at the pivot of the initial *G*-axis. Possible virtual complexes were generated by sequential pivoting on *X*, *Y*, and variable *G*, with 5° steps. The *G*-axis was first set by rotations on the *Y*-axis with angle β ($0 \leq \beta < 360°$), and on the *X*-axis with angle α ($0 \leq \alpha < 180°$). The ligand was then rotated on the *G*-axis by angle γ ($0 \leq \gamma < 360°$). 3D structures were illustrated by the general three-dimensional transformation method (*25*). Derived complex models were scored by the number of conflicting atom pairs based on the atomic distance between PP1 and the ligand. Atom pairs were defined as conflicting when the distance was below 2.9 Å (C-C), 2.7 Å (C-O), 2.8 Å (C-N), 2.6 Å (O-O), 2.6 Å (O-N), or 2.6 Å (N-N), based on the experimental data from the crystal structures (*26*). Molecules were treated as rigid bodies during the modeling. In PP1·CPI-17 modeling, we prescreened the library using violation on the atomic distance between main chains with a threshold of 3.5 Å (Cα-Cα), or 2.0 Å (N-O, N-N, O-O). The phospho-pivot modeling program was executed on a single 2 GHz processor of Apple Power Mac G5 computer under Mac OS 10.3.4.

Energy Minimization—Energy minimization was performed with permission of structural change of both molecules using the AMBER force field on SYBYL/BIOPOLYMER (Tripos Inc.).

Binding Assay—His_6-S–tagged CPI-17 was prepared and thiophosphorylated with ATPγS, as described previously (*15*). GST-MYPT1(1–300) was prepared from a bacterial lysate. The cDNA fragment encoding human MYPT1(1–300) was prepared by PCR method and inserted at *Bam*H1/*Eco*RI site of pGEX-4T-2 vector. Bacteria BL21(DE3) transformed with the vector DNA was harvested overnight at 37°C in 10 ml of Luria-Bertani (LB) broth with 100 μg/ml ampicillin and 0.8% glucose. The culture was added into 400 ml of fresh LB broth with 100 μg/ml ampicillin and 2% EtOH. After a 2-h incubation at 37°C, the recombinant protein expression was induced for 24 h at 23°C by addition of 0.1 mM isopropyl b-D-1-thiogalactopyranoside. Cells were collected by centrifugation and subjected to a freeze-and-thaw process in the presence of 1 mg/ml lysozyme (Sigma L-6876). The lysate was clarified for 1 h at 100,000 × *g* and the GST-fusion protein in the supernatant was purified by glutathione-agarose (Sigma G-4510) affinity chromatography according to the manufacturer's protocol. The coding region of pig PP1 delta cDNA was inserted in pHA_3 mammalian expression vector downstream of a CMV promoter/enhancer element sequence. Point mutation of the cDNA was performed by Quikchange™ technique from Stratagene. $(HA)_3$-PP1 delta was transiently expressed for 24 h in COS7 cells in a 100 mm dish using FuGene6™ reagent (Roche Applied Science). Cells were lysed with 1 ml of lysis buffer [50 mM Tris-HCl (pH 8.0), including 0.2 M NaCl, 1 mM EGTA, 1% Triton X-100, 0.4 mM Pefabloc™, 10 μg/ml trypsin inhibitor, and 0.1% 2-mercaptethanol]. The homogenate was clarified by a centrifugation for 20 min at 4°C, and the supernatant was split into three portions. An aliquot (50 μl) was mixed with 2× Laemmli sample buffer, 0.5 ml was mixed with S-protein™ agarose (Novagen) conjugated with thiophospho-His6-S-CPI-17 (5 μg), and 0.5 ml was mixed with glutathione-agarose (Sigma) conjugated with GST-MYPT1(1–300) (10 μg). After a 90-min incubation at 4°C, resins were collected by brief centrifugation and were washed 3 times with lysis buffer. Proteins bound to the ligand were released with 20 μl of Laemmli sample buffer and subjected to immunoblotting. HA-PP1 delta was detected on X-lay film using Supersignal™ reagent (Pierce) with anti-HA antibody (0.1 μg/ml). The HA signal on the film was quantified using Densitometer (Molecular probe). Protein determination and immunoblotting were done as described previously (*15*).

RESULTS

Phospho-Pivot Modeling—The initial step in the phospho-pivot modeling strategy positions the phosphate group of the ligand at the docking site on the phosphoreceptor, in this case P-Thr38 at the PP1 active site. The modeling consists of two stages; 1st is to generate a series of virtual complexes by pivoting the ligand on a receptor protein at the phosphate, and 2nd is to score and grade these complexes based on atomic proximity of the opposing surfaces of the two molecules. Because the pivot is pre-set at the docking site, the phospho-pivot modeling method does not require the step of searching for unmapped docking sites over the entire surface as done under conventional modeling algorithms. This greatly reduces the computational tasking and enables a personal computer to handle it. To test this novel approach, we applied it to modeling PP1·calyculin A complex, which has been co-crystallized previously (*27*) (PDB: 1IT6). Calyculin A is a phospho-polyketide inhibitory compound isolated from marine sponge and the phosphate group of calyculin A is critical for potent interaction with PP1 (*28*), which mimics a phosphate of substrates at the active site of protein phosphatases formed with a bimetal center (*27*).

In the PP1·calyculin A modeling, calyculin A was pivoted at the phosphorus atom in 5°steps on the *X*, *Y* and *G* axes in range of $0 \leq \alpha < 180°$, $0 \leq \beta < 360°$ and $0 \leq \gamma < 360°$ (Fig. 1A). This three-axis pivoting yielded $36 \times 72 \times 72 = 186{,}624$ models of the complex. Initial orientation of calyculin A did not affect the results (data not shown). The number of conflicting atom pairs were then scored to grade the derived complex models. Figure 1B shows distribution of the number of conflicts, where groups with the fewest conflicts are indicated in red, cyan and blue. Models with a conflict number < 20 were selected, and their relative rotational angles are plotted in Fig. 1C. Models with the fewest conflicts distributed on 2 clusters in the α/β angle map and on 4 clusters in α/γ angle map, indicating that the restriction on the atomic distances allowed limited orientations of calyculin A against PP1 (Fig. 1C). Models in the top 20 with the fewest conflicts (red) were found only in one cluster with $0 \leq \alpha \leq 20°$ on the *X*-axis, $320 \leq \beta \leq 345°$ on the *Y*-axis and $340° \leq \gamma \leq 15°$ on the *G*-axis. AMBER force energy calculation was performed for the representative models in each clusters (Table 1). The estimated binding energy is lower in the model including fewer conflicts (Table 1). Therefore, we used number of conflicts to evaluate the structure of the

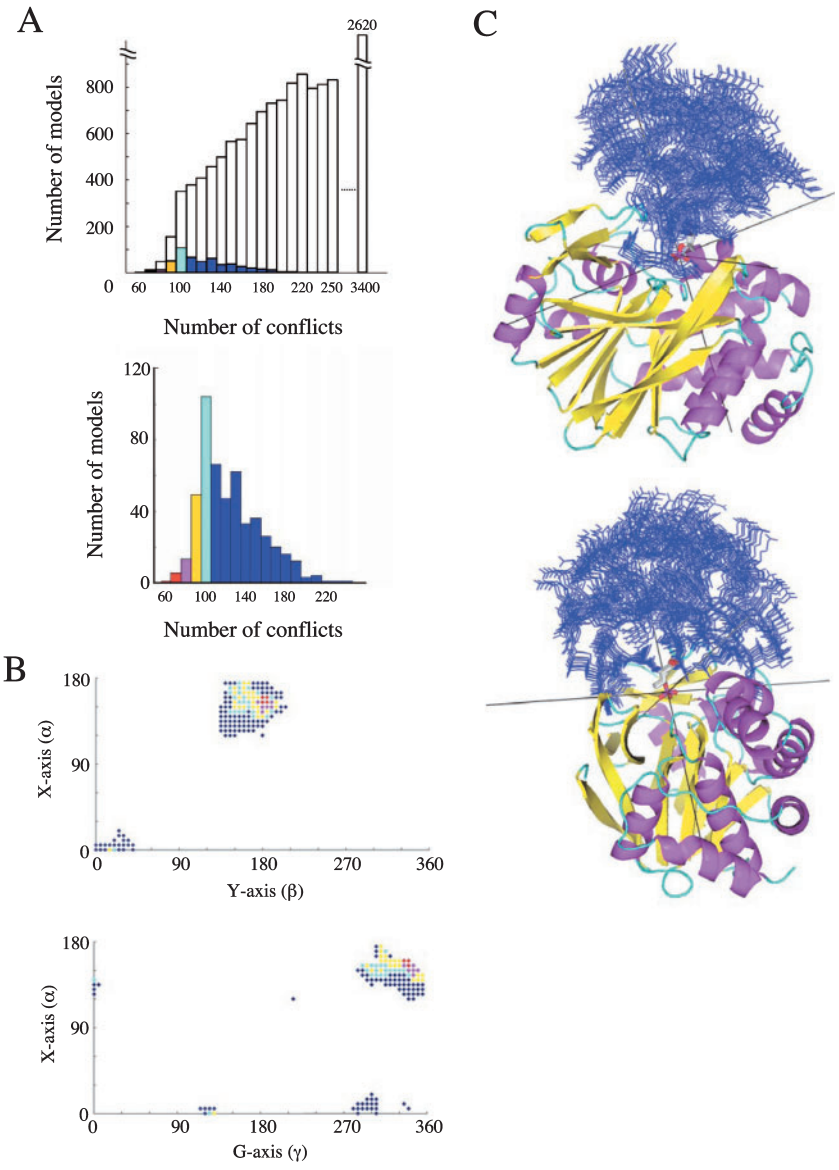

Fig. 2. **Modeling of PP1·P-CPI-17 complex.** (A) Distribution of PP1·P-CPI-17 models by conflict number. Models passing the initial filtering on restriction of main chain atomic distance are shown in colored bars. Conflict number, 1–69, 70–79, 80–89, 90–99 and 100–239 are indicated in red, magenta, cyan, and blue, respectively. (B) Distribution of models in angle map. Each spot indicates a model with the color as in panel A. Top and bottom panels show angle maps of X/*Y* and *X*/*G* axes, respectively. (C) Superimposed structure of PP1·P-CPI-17 complex. Structures of CPI-17 in top 10 models with conflict numbers less than 74 are shown with blue lines. Bottom structure shows 90°-rotated form from top. The structure was drawn using PyMoL (*43*).

model. Figure 1D illustrates superimposed structures of calyculin A on PP1 for the top 10 models with conflict numbers below 2. Orientation of calyculin A in these models is essentially identical to X-ray crystallographic structure indicated as the red structure in Fig. 1D. Calyculin A in the model was fit to that in the crystal structure, where the lowest r.m.s.d. value for all atoms was 0.23 Å. Thus, the phosphate-pivot modeling is sufficient to predict the interface in protein·ligand complex. This modeling was done within a 40-min computation. A lower step angle value such as 3°, reduced the lowest r.m.s.d. value of the model in the library, but it increased the number of models in the library, which caused over 10-fold increase in the computation time (421 min).

Modeling of PP1·CPI-17 Complex—Because P-CPI-17 structure was not available, the coordinate data of T38D form of CPI-17 mimicking the active conformation (*24*) were used for the modeling, with a virtual substitution from Asp 38 to phospho-Thr. The virtual phosphate of P-CPI-17 was set at the position of the phosphate in the calyculin A molecule, and 186,624 models were generated by the pivoting. Models, which have conflicts between main chain atoms of two proteins, were neglected from the grading process. After the pre-screening process, 499 complex models were selected and subjected to the all-atomic grading with the same parameters used for the calyculin A complex. The distribution of PP1·P-CPI-17 models with the number of conflicts shows bell shape peaking at 90–100 conflicts (red/magenta/cyan/blue bar in Fig. 2A), indicating that the pre-screening process effectively eliminated models with a high number of conflicts (Fig. 2A white portion). These models formed one dominant cluster in the angle map (Fig. 2B). Red dots indicate the 18 models with the fewest conflicts of 59–79, and were found only in the dominant cluster. They distributed in narrow range of α/β/γ angles, within 15° (Fig. 2B) that reflects a limited orientation of CPI-17 against PP1, as shown in the superimposed structures of top-10 models (Fig. 2C, blue lines). Main chain atoms of the inhibitory P-loop in each top-10 model were positioned with average r.m.s.d. of 1.1 Å. This modeling was done

Table 1. **Correlation between number of conflicts and the estimated binding energy of PP1·calyculin A complex.**

Cluster	Angle (*a, b, g*) (°)	Number of conflict	Binding energy (kcal/mol)
1	10, 330, 0	1	–6,358
2	170, 145, 355	7	–6,313
3	5, 15, 140	10	–6,276
4	120, 165, 115	19	–6,274

Representative models of each cluster (#1–4) in Fig. 1C were subjected to AMBER energy calculation.

with a 400-min processing, whereas it took for 1,283 min without the pre-screening process (*29*).

Structure of PP1·P-CPI-17 Complex—All 18 models with the fewest conflicts of 59–79 (red/magenta bar in Fig. 3A) were processed to AMBER force energy refinement with permission of structural change on both CPI-17 and PP1 structure to minimize conformational energy. Figure 3 illustrates a model with the lowest energy value after a 100-step energy refinement on the 18 models. The model underwent conformational changes with the main-chain r.m.s.d. value of 0.33 Å from the original model. The ridge formed by the inhibitory P-loop in P-CPI-17 fits along the active site groove of PP1 (Fig. 3A). Along with the P-loop in the groove, helices A and B of CPI-17 are in close proximity to the surface of PP1 adjacent to the active site groove. The curvature of the P-loop fits in the active site groove of PP1 (Fig. 3B). The main chain of CPI-17 between P-Thr38 and Arg44 overlaps with calyculin A in the hydrophobic cluster of PP1 (Fig. 3B, right). On the other hand, the segment between Arg33–Val37 of CPI-17 lies near the β12–13 loop of PP1, unlike calyculin A, whose an oxazole ring sits at the acidic groove of PP1.

A Ser/Thr phosphatase, calcineurin (CaN, PP2B), consists of a globular domain with the active site and a tail domain with an autoinhibitory segment. The autoinhibitory domain (CaN 469–486) docks at the active site of

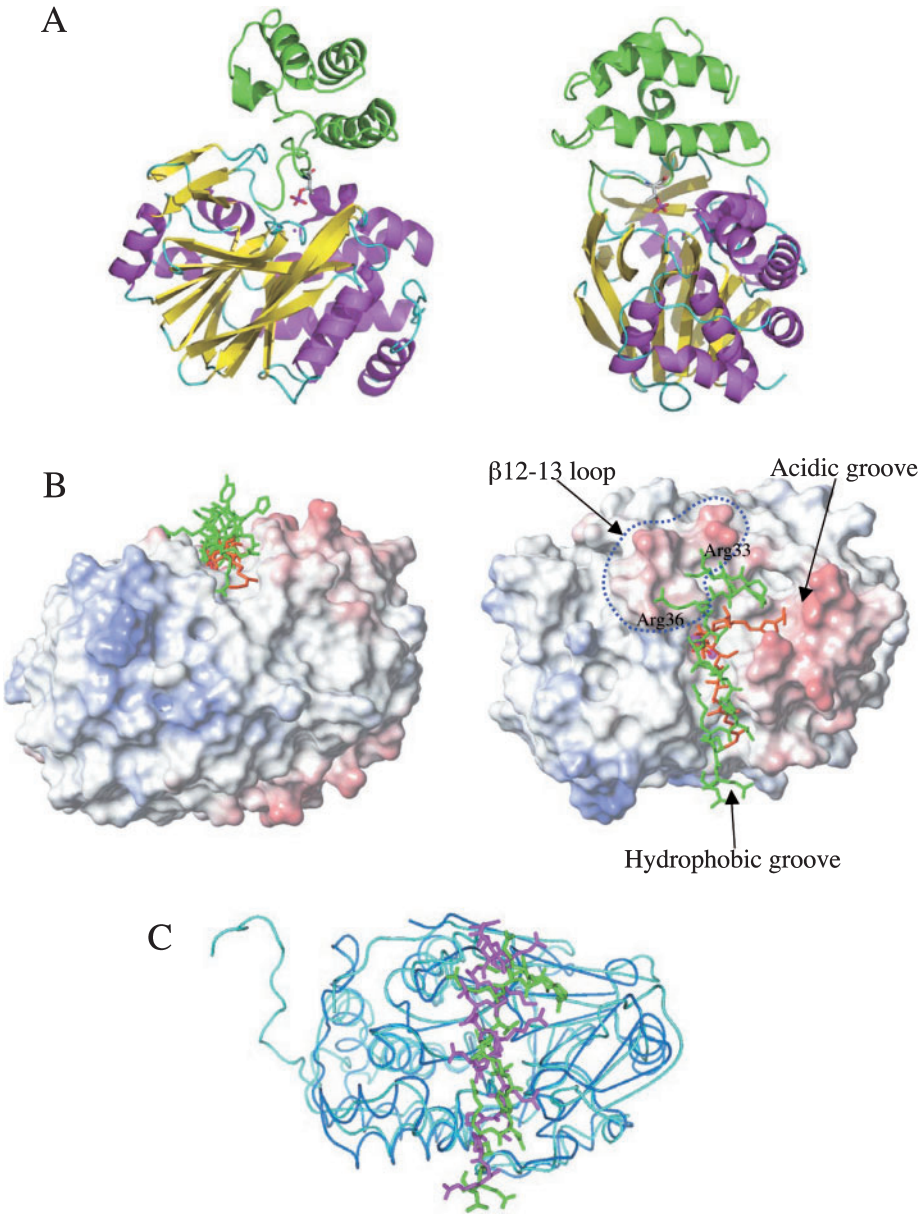

Fig. 3. **Best fit model of the PP1·P-CPI-17 complex.** (A) PP1·P-CPI-17 complex. The view from the hydrophobic groove of PP1 (left) and its 90° rotated view of the complex model with one conflict is shown with the entire structure of CPI-17 PHIN domain (green). A pair of dots indicates Mn^{2+} ion at the active site of PP1, and the phosphate group is indicated in red. (B) Location of P-loop of CPI-17 on the PP1 surface. The PP1 surface was calculated using SYBYL/MOLCAD (Tripos Inc.), where red and blue indicate negative and positive charged regions, respectively. P-loop, a segment from Gln31 to Leu46, of CPI-17 is in green, and calyculin A is in orange. Left view corresponds to panel A left. The active site of PP1 is set on the front in the right view. (C) Comparison between structures of CaN·autoinhibitory domain and PP1·CPI-17 P-loop. The structure of the catalytic domain of CaN (1–350) (cyan) (PDB : 1AUI) was superimposed with PP1 structure (blue) of the PP1·P-CPI-17 complex. The autoinhibitory domain of CaN (469–486) and CPI-17 P-loop are shown in purple and green, respectively.

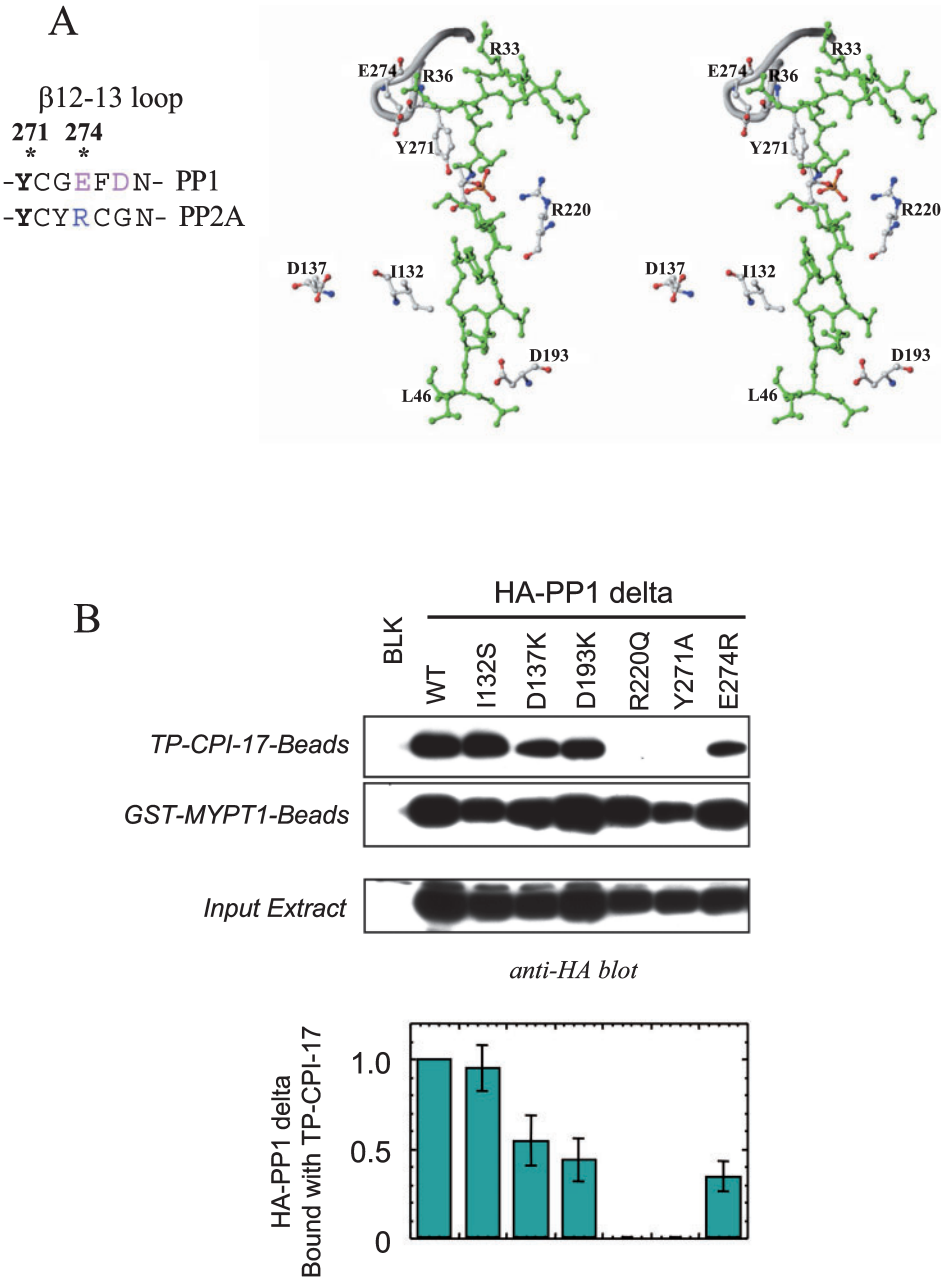

Fig. 4. **Interface of PP1 against P-CPI-17.** (A) Stereo view of P-loop of CPI-17 and surrounding side chains of PP1. P-loop of CPI-17 (Gln31–Leu46) with side chains is colored green and the phosphate is red. Main chain of β12–13 loop is illustrated as a gray tube. Red and blue in PP1 side chains are nitrogen and oxygen atoms, respectively. Inset: Sequence alignment in β12–13 loop of PP1 and PP2A. (B) Binding assay of P-CPI-17 with HA-PP1 mutants. HA-PP1 delta WT and mutants were transiently expressed in COS7 cells. The cell lysate was mixed with resins conjugated with thiopospho-CPI-17 (TP-CPI-17) or MYPT1(1–300) PP1 binding fragment. The bound HA-PP1 was detected by immunoblotting with anti-HA antibody. TP-CPI-17-bound HA-PP1 was quantified using densitometry of the blot. Mean values and SEM from three independent experiments are shown in the bar graph.

CaN in the X-ray crystal structure (*30*). Figure 3C illustrates the relative positions of the autoinhibitory domain of CaN (purple) and the inhibitory P-loop of CPI-17 (green) on the active site of CaN and PP1. The structure of CaN catalytic domain is very similar to that of PP1. Interestingly, although CaN autoinhibitory domain forms an alpha helix, unlike the P-loop of CPI-17, the position of both segments is converged on the cleft of the active site along the β12–13 loop, and their directions are identical. The mechanism of inhibition may be conserved between CaN and PP1 as active site structures of both enzymes are conserved.

Interface of PP1·P-CPI-17 Complex—The phosphate group of CPI-17 was set at the active site in the place of the phosphate of calyculin A, which is clamped between Arg220 and Tyr271 of PP1 (Fig. 4A). In agreement with the structure of PP1·calyculin A complex, mutational studies demonstrated that Arg220 (221 in alpha isoform) plays critical roles in the hydrolysis of the phospho-substrate (*27*, *31*). In addition, mutation at Tyr271 (272 in alpha) was reported to reduce V_{max} and to increase IC50 values against inhibitor compounds, including calyculin A and DARPP32 (*32*, *33*). Tyr271 is located in the β12–13 loop of PP1, which forms a protrusion overhanging the active site (Fig. 3B, right). Tyr271 is conserved in Ser/Thr phosphatase family, whereas the following sequence, GEFD in PP1, is characteristic and negatively charged in PP1 (Fig. 4A, inset). By chimeric mutational studies on PP1 and PP2A, Zhang *et al.* showed that the segment GEFD of PP1 determines sensitivities to okadaic acid and inhibitor-2 (*34*). In our model, guanidium groups of Arg33 and 36 in CPI-17 are in close proximity to Glu274/

Asp276 in the GEFD segment (Figs. 3B and 4A). In the hydrophobic groove of PP1, Ile131 has been reported to interact with microcystin LR and okadaic acid (*14*, *35*), although no hydrophobic residues of CPI-17 are close to the hydrophobic cluster. Another salt bridge between Arg44 of CPI-17 and Asp193 of PP1 is evident at the edge of the hydrophobic groove in this model, although no significant contribution of Asp193 to the interaction with inhibitor compounds was reported in the previous crystal structures. In addition to the P-loop, A-helix of CPI-17 locates over the N-terminal subdomain of PP1, outside the active site (Fig. 4). Especially Lys55 of CPI-17 is 4.6 Å away from Asp137 of PP1, suggesting a potential salt bridge.

Binding Assay of P-CPI-17 with PP1—To evaluate this model, we tested interactions of P-CPI-17 with recombinant PP1 mutants. Unlike native protein, bacterial recombinant PP1 requires Mn^{2+} ion for the activity and lacks sensitivity against inhibitor-1 and DARPP32 (*36*, *37*). Indeed, P-CPI-17 is dephosphorylated by the bacterial PP1 protein (data not shown). Therefore, we expressed HA-tagged PP1 delta isoform in COS7 cells and used the lysate as the PP1 preparation in a binding assay. The cell lysates including HA-PP1 mutants were mixed with thiophospho-CPI-17 coupled beads and the bound HA-PP1 was detected by immunoblotting using anti-HA antibody (Fig. 4B, top and bottom panels). Each sample included equivalent amounts of HA-PP1 WT and mutants (Fig. 4B, input extract). PP1 mutants maintain the allosteric interaction with GST-MYPT1(1–300) fragment, suggesting no disruption in overall conformation by these mutations (Fig. 4B, GST-MYPT1 bound). Mutations at Arg220 or Tyr271 completely eliminated the binding with TP-CPI-17. The results strongly support our initial hypothesis that the phosphate of P-CPI-17 docks directly at the active site of PP1. The E274R mutant mimicking PP2A sequence in the β12–13 loop lost its affinity for TP-CPI-17. Similarly point mutations at Asp137 or 193 of PP1 reduce binding to TP-CPI-17. Compared with D137K, D193K, or E274R mutant, the mutation at Arg220 or Tyr271 was more effective on the interaction with P-CPI-17. On the other hand, substitution of Ile132 in the hydrophobic groove to Ser does not affect on the interaction with TP-CPI-17. Thus the mutational analysis data are consistent with the structure of PP1·P-CPI-17 complex predicted by the phospho-pivot modeling.

DISCUSSION

Phospho-pivot modeling is based on the hypothesis that phosphorylated residues in proteins serve as dominant recognition elements for protein–protein association. Advantage of the phospho-pivot modeling is to project the molecular complex image, easily and quickly at our desk. Although it cannot describe details of the molecular interface, the information from the modeling was sufficient to design site-specific mutants of PP1. This easy modeling method is expected to fill a gap in structural biology. One example is the direct binding of the phosphate of CPI-17 with the active site of PP1. Previous data showed that replacing Thr38 of CPI-17 with Asp does not enhances the affinity for PP1, even though the solution conformation of the Asp38 mutant is very similar to the phospho-form (*24*). Indeed the mutation at the phosphate-binding residues of PP1 Arg220/Tyr271 completely eliminate the interaction with P-CPI-17. Thus, the phosphorylation of CPI-17 at Thr38 induces the active conformation of the protein, and the phosphate functions as a coupler docking at the active site of PP1.

Structural data on oligomeric protein complexes are accumulating in Protein Data Bank provided by structural biologists using X-ray crystalographic and/or NMR spectroscopic techniques (*3*). P-CPI-17 is easily dephosphorylated by recombinant PP1, and even thiophospho-CPI-17 is partially hydrolyzed under conditions used for structural studies (data not shown); therefore, we could not obtain a stable complex of PP1·P-CPI-17 *in vitro*. Our phospho-pivot modeling enables us to visualize the 3D structure of this fragile phospho-protein complex in silico. Initial modeling was done assuming two rigid molecules. Models of PP1·P-CPI-17 complex include at least 59 conflicts in their structures, implying alimitation of this simple modeling algorithm in simulating the molecular interface. Nonetheless, it is possible that the model demonstrates an initial collision between two molecules, unlike X-ray co-crystal structure, which represents a stabilized conformation. The initial conflicts found in this modeling may drive conformational changes to reach an energy minimum structure. Thus, comparison of the structures from the phosphate-pivot modeling and the X-ray co-crystal structure would help in understanding how the conformational change undergoes after molecular collisions. Because P-CPI-17 acts as an inhibitor and a substrate of PP1 (*23*), the modeled PP1·P-CPI-17 complex possibly represents the structure of pre-Michaelis-Menten complex (pre-ES complex) of PP1 and the substrate. Recently Brinkworth et al reported 3D structure-based prediction of substrate specificity in protein kinases (*38*). The phospho-pivot modeling is capable of revealing PP1·P-substrate interfaces that will uncover rules of substrate specificity in Ser/Thr phosphatases.

The hydrophobic groove of PP1 is not involved in the interaction with P-CPI-17 unlike the interaction with other inhibitor compounds (*14*, *27*, *35*). Thus, electrostatic interactions rather than hydrophobic interaction seem to be dominant in the PP1·P-CPI-17 complex, which is consistent with our previous finding that myosin phosphatase is eluted from TP-CPI-17 affinity resin with moderate salt concentration of 0.5 M NaCl (*39*). Furthermore, the phospho-pivot modeling successfully predicts the interaction of P-CPI-17 with Glu274 in PP1 β12–13 loop, where the amino acid sequence is unique to PP1 among the Ser/Thr phosphatase family. P-CPI-17 does not inhibit purified PP2A or calcineurin (*40*). The interaction with β12–13 loop is suggested to be a determinant for the specificity of CPI-17. However the mutation at Glu274 did not completely eliminate the affinity for P-CPI-17. P-CPI-17 might recognize the overall conformation of PP1 as well as the residues in β12–13 loop. For this modeling, we used structures of T38D-CPI-17, which mimics that of P-form but does not bind recombinant PP1. Nonetheless, the predicted structure is sufficient to guide mutational analyses on the interaction. During the preparation of this manuscript, the co-crystal structure

of the PP1·MYPT1 fragment was reported (*41*). The position of CPI-17 in our model does not conflict with the MYPT1 fragment in the complex, where MYPT1 docks at the back side of the active site (data not shown). Further structural data for phosphorylated CPI-17 are expected to refine the modeling data of the MYPT1·PP1·P-CPI-17 complex.

Furthermore, we are expecting that the phospho-pivot modeling will be applied to proteins consisting of phosphate receptors, such as 14–3-3 protein and BRCA1 BRCT domain (*1*, *42*). Small phospho-peptide, phospho-compounds, sulfate, or tungstate ions have been co-crystallized with phosphate receptor proteins. We expect that these phosphate or analog ions provide us the position of the pivot for modeling. Half of human proteins, over 25,000, are predicted to be phospho-proteins. The phospho-pivot modeling will provide a powerful tool for their analysis in post-genomic era.

We thank Prof. David L. Brautigan, University of Virginia, for his enthusiastic support and for proofreading this manuscript.

REFERENCES

1. Yaffe, M.B. and Smerdon, S.J. (2004) The use of in vitro peptide-library screens in the analysis of phosphoserine/threonine-binding domain structure and function. *Annu. Rev. Biophys Biomol. Struct.* **33**, 225–244
2. Pawson, T. (1995) Protein modules and signalling networks. *Nature* **373**, 573–580
3. Jones, S. and Thornton, J.M. (1996) Principles of protein-protein interactions. *Proc. Natl Acad. Sci. USA* **93**, 13–20
4. Uetz, P., Giot, L., Cagney, G., Mansfield, T.A., Judson, R.S., Knight, J.R., Lockshon, D., Narayan, V., Srinivasan, M., Pochart, P., Qureshi-Emili, A., Li, Y., Godwin, B., Conover, D., Kalbfleisch, T., Vijayadamodar, G., Yang, M., Johnston, M., Fields, S., and Rothberg, J.M. (2000) A comprehensive analysis of protein-protein interactions in *Saccharomyces cerevisiae*. *Nature* **403**, 623–627
5. Ito, T., Chiba, T., Ozawa, R., Yoshida, M., Hattori, M., and Sakaki, Y. (2001) A comprehensive two-hybrid analysis to explore the yeast protein interactome. *Proc. Natl Acad. Sci. USA* **98**, 4569–4574
6. Giot, L., Bader, J.S., Brouwer, C., Chaudhuri, A., Kuang, B., Li, Y., Hao, Y.L., Ooi, C.E., Godwin, B., Vitols, E., Vijayadamodar, G., Pochart, P., Machineni, H., Welsh, M., Kong, Y., Zerhusen, B., Malcolm, R., Varrone, Z., Collis, A., Minto, M., Burgess, S., McDaniel, L., Stimpson, E., Spriggs, F., Williams, J., Neurath, K., Ioime, N., Agee, M., Voss, E., Furtak, K., Renzulli, R., Aanensen, N., Carrolla, S., Bickelhaupt, E., Lazovatsky, Y., DaSilva, A., Zhong, J., Stanyon, C.A., Finley, R.L., Jr., White, K.P., Braverman, M., Jarvie, T., Gold, S., Leach, M., Knight, J., Shimkets, R.A., McKenna, M.P., Chant, J., and Rothberg, J.M. (2003) A protein interaction map of *Drosophila melanogaster*. *Science* **302**, 1727–1736
7. Li, S., Armstrong, C.M., Bertin, N., Ge, H., Milstein, S., Boxem, M., Vidalain, P.O., Han, J.D., Chesneau, A., Hao, T., Goldberg, D.S., Li, N., Martinez, M., Rual, J.F., Lamesch, P., Xu, L., Tewari, M., Wong, S.L., Zhang, L.V., Berriz, G.F., Jacotot, L., Vaglio, P., Reboul, J., Hirozane-Kishikawa, T., Li, Q., Gabel, H.W., Elewa, A., Baumgartner, B., Rose, D.J., Yu, H., Bosak, S., Sequerra, R., Fraser, A., Mango, S.E., Saxton, W.M., Strome, S., Van Den Heuvel, S., Piano, F., Vandenhaute, J., Sardet, C., Gerstein, M., Doucette-Stamm, L., Gunsalus, K.C., Harper, J.W., Cusick, M.E., Roth, F.P., Hill, D.E., and Vidal, M. (2004) A map of the interactome network of the metazoan *C. elegans*. *Science* **303**, 540–543
8. Smith, G.R. and Sternberg, M.J. (2003) Evaluation of the 3D-Dock protein docking suite in rounds 1 and 2 of the CAPRI blind trial. *Proteins* **52**, 74–79
9. Elcock, A.H., Sept, D., and McCammon, J.A. (2001) Computer simulation of protein-protein interactions. *J. Phys. Chem. B* **105**, 1504–1518
10. Gray, J.J., Moughon, S.E., Kortemme, T., Schueler-Furman, O., Misura, K.M., Morozov, A.V., and Baker, D. (2003) Protein-protein docking predictions for the CAPRI experiment. *Proteins* **52**, 118–122
11. Chen, R., Tong, W., Mintseris, J., Li, L., and Weng, Z. (2003) ZDOCK predictions for the CAPRI challenge. *Proteins* **52**, 68–73
12. Fernandez-Recio, J., Totrov, M., and Abagyan, R. (2004) Identification of protein-protein interaction sites from docking energy landscapes. *J. Mol. Biol.* **335**, 843–865
13. Fernandez-Recio, J., Totrov, M., and Abagyan, R. (2003) ICM-DISCO docking by global energy optimization with fully flexible side-chains. *Proteins* **52**, 113–117
14. Goldberg, J., Huang, H.B., Kwon, Y.G., Greengard, P., Nairn, A.C., and Kuriyan, J. (1995) Three-dimensional structure of the catalytic subunit of protein serine/threonine phosphatase-1. *Nature* **376**, 745–753
15. Eto, M., Leach, C., Tountas, N.A., and Brautigan, D.L. (2003) Phosphoprotein inhibitors of protein phosphatase-1 in *Methods Enzymol.* (Klumpp, S. and Krieglstein, J., eds.) pp. 243–260, Academic Press, San Diego
16. Eto, M., Ohmori, T., Suzuki, M., Furuya, K., and Morita, F. (1995) A novel protein phosphatase-1 inhibitory protein potentiated by protein kinase C. Isolation from porcine aorta media and characterization. *J. Biochem.* **118**, 1104–1107
17. Eto, M., Bock, R., Brautigan, D., and Linden, D.J. (2002) Cerebellar long-term synaptic depression requires PKC-mediated activation of CPI-17, a myosin/moesin phosphatase inhibitor. *Neuron* **36**, 1145–1158
18. Kitazawa, T., Polzin, A., and Eto, M. (2004) CPI-17-Deficient Smooth Muscle of Chicken. *J. Physiol.* **557**, 515–528
19. Somlyo, A.P. and Somlyo, A.V. (2003) Ca^{2+} sensitivity of smooth muscle and nonmuscle myosin II: modulated by G proteins, kinases, and myosin phosphatase. *Physiol. Rev.* **83**, 1325–1358
20. Ohki, S., Eto, M., Kariya, E., Hayano, T., Hayashi, Y., Yazawa, M., Brautigan, D., and Kainosho, M. (2001) Solution NMR structure of the myosin phosphatase inhibitor protein CPI- 17 shows phosphorylation-induced conformational changes responsible for activation. *J. Mol. Biol.* **314**, 839–849
21. Kitazawa, T., Eto, M., Woodsome, T.P., and Brautigan, D.L. (2000) Agonists trigger G protein-mediated activation of the CPI-17 inhibitor phosphoprotein of myosin light chain phosphatase to enhance vascular smooth muscle contractility. *J. Biol. Chem.* **275**, 9897–9900
22. Pang, H., Guo, Z., Su, W., Xie, Z., Eto, M., and Gong, M.C. (2005) RhoA/Rho kinase mediates thrombin- and U-46619-induced phosphorylation of a myosin phosphatase inhibitor, CPI-17, in vascular smooth muscle cells. *Am. J. Physiol., Cell Physiol.* (in press)
23. Eto, M., Kitazawa, T., and Brautigan, D.L. (2004) Phosphoprotein inhibitor CPI-17 specificity depends on allosteric regulation of protein phosphatase-1 by regulatory subunits. *Proc. Natl Acad. Sci. USA (Track II)* **101**, 8888–8893
24. Ohki, S., Eto, M., Shimizu, M., Takada, R., Brautigan, D.L., and Kainosho, M. (2003) Distinctive solution conformation of phosphatase inhibitor CPI-17 substituted with asparatate at the phosphorylation-site threonine residues. *J. Mol. Biol.* **326**, 1539–1547
25. Foley, J.D., van Dam, A., Feiner, S.K., and Hughes, J.F. (1996) *Computer Graphics: Principles and Practice in C*, 2nd ed., Addison-Wesley Professional
26. Ramachandran, G.N. and Sasisekharan, V. (1968) Conformation of polypeptides and proteins. *Adv. Protein Chem.* **23**, 283–438
27. Kita, A., Matsunaga, S., Takai, A., Kataiwa, H., Wakimoto, T., Fusetani, N., Isobe, M., and Miki, K. (2002) Crystal structure

of the complex between calyculin A and the catalytic subunit of protein phosphatase 1. *Structure (Camb.)* **10**, 715–724
28. Wakimoto, T., Matsunaga, S., Takai, A., and Fusetani, N. (2002) Insight into binding of calyculin A to protein phosphatase 1: isolation of hemicalyculin a and chemical transformation of calyculin A. *Chem. Biol.* **9**, 309–319
29. Matsuzawa, F., Ohki, S., Aikawa, S., and Eto, M. (2005) Computational simulation for interaction of nano-molecules: The phospho-pivot modeling algorithm for prediction of interactions between a phospho-protein and its receptor. *Sci. Technol. Adv. Mater.* (in press)
30. Kissinger, C.R., Parge, H.E., Knighton, D.R., Lewis, C.T., Pelletier, L.A., Tempczyk, A., Kalish, V.J., Tucker, K.D., Showalter, R.E., Moomaw, E.W., Louis, N.G., Habuka, N., Chen, X.M., Maldonado, F., Barker, J.E., Bacquet, R., and Villafranca, J.E. (1995) Crystal structures of human calcineurin and the human FKBP12-FK506-calcineurin complex. *Nature* **378**, 641–644
31. Zhang, L. and Lee, E.Y. (1997) Mutational analysis of substrate recognition by protein phosphatase 1. *Biochemistry* **36**, 8209–8214
32. Zhang, L., Zhang, Z., Long, F., and Lee, E.Y. (1996) Tyrosine-272 is involved in the inhibition of protein phosphatase-1 by multiple toxins. *Biochemistry* **35**, 1606–1611
33. Watanabe, T., Huang, H.B., Horiuchi, A., da Cruze Silva, E.F., Hsieh-Wilson, L., Allen, P.B., Shenolikar, S., Greengard, P., and Nairn, A.C. (2001) Protein phosphatase 1 regulation by inhibitors and targeting subunits. *Proc. Natl Acad. Sci. USA* **98**, 3080–3085
34. Zhang, Z., Zhao, S., Long, F., Zhang, L., Bai, G., Shima, H., Nagao, M., and Lee, E.Y. (1994) A mutant of protein phosphatase-1 that exhibits altered toxin sensitivity. *J. Biol. Chem.* **269**, 16997–17000
35. Maynes, J.T., Bateman, K.S., Cherney, M.M., Das, A.K., Luu, H.A., Holmes, C.F., and James, M.N. (2001) Crystal structure of the tumor-promoter okadaic acid bound to protein phosphatase-1. *J. Biol. Chem.* **276**, 44078–44082
36. Endo, S., Connor, J.H., Forney, B., Zhang, L., Ingebritsen, T.S., Lee, E.Y., and Shenolikar, S. (1997) Conversion of protein phosphatase 1 catalytic subunit to a Mn^{2+}-dependent enzyme impairs its regulation by inhibitor 1. *Biochemistry* **36**, 6986–6992
37. Watanabe, T., da Cruz e Silva, E.F., Huang, H.B., Starkova, N., Kwon, Y.G., Horiuchi, A., Greengard, P., and Nairn, A.C. (2003) Preparation and characterization of recombinant protein phosphatase 1. *Methods Enzymol.* **366**, 321–338
38. Brinkworth, R.I., Breinl, R.A., and Kobe, B. (2003) Structural basis and prediction of substrate specificity in protein serine/threonine kinases. *Proc. Natl Acad. Sci. USA* **100**, 74–79
39. Senba, S., Eto, M., and Yazawa, M. (1999) Identification of trimeric myosin phosphatase (PP1M) as a target for a novel PKC-potentiated protein phosphatase-1 inhibitory protein (CPI17) in porcine aorta smooth muscle. *J. Biochem.* **125**, 354–362
40. Eto, M., Senba, S., Morita, F., and Yazawa, M. (1997) Molecular cloning of a novel phosphorylation-dependent inhibitory protein of protein phosphatase-1 (CPI17) in smooth muscle: Its specific localization in smooth muscle. *FEBS Lett.* **410**, 356–360
41. Terrak, M., Kerff, F., Langsetmo, K., Tao, T., and Dominguez, R. (2004) Structural basis of protein phosphatase 1 regulation. *Nature* **429**, 780–784
42. Clapperton, J.A., Manke, I.A., Lowery, D.M., Ho, T., Haire, L.F., Yaffe, M.B., and Smerdon, S.J. (2004) Structure and mechanism of BRCA1 BRCT domain recognition of phosphorylated BACH1 with implications for cancer. *Nat. Struct. Mol. Biol.* **11**, 512–518
43. De Lano, W.L. (2002) *The PyMOL Molecular Graphics System*, DeLano Scientific, San Carlos, CA